JACS
JOURNAL OF THE AMERICAN CHEMICAL SOCIETY

Article

pubs.acs.org/JACS

Mechanistic Studies on Initiation and Propagation of Rare Earth Metal-Mediated Group Transfer Polymerization of Vinylphosphonates

Stephan Salzinger, Benedikt S. Soller, Andriy Plikhta, Uwe B. Seemann, Eberhardt Herdtweck, and Bernhard Rieger*

WACKER-Lehrstuhl für Makromolekulare Chemie, Technische Universität München, Lichtenbergstraße 4, 85748 Garching bei München, Germany

Supporting Information

ABSTRACT: Initiation of rare earth metal-mediated vinylphosphonate polymerization with unbridged rare earth metallocenes (Cp_2LnX) follows a complex reaction pathway. Depending on the nature of X, initiation can proceed either *via* abstraction of the acidic α-CH of the vinylphosphonate (e.g., for X = Me, CH_2TMS), *via* nucleophilic transfer of X to a coordinated monomer (e.g., for X = Cp, SR) or *via* a monomer (i.e., donor)-induced ligand-exchange reaction forming Cp_3Ln in equilibrium (e.g., for X = Cl, OR), which serves as the active initiating species. As determined by mass spectrometric end group analysis, different initiations may also occur simultaneously (e.g., for X = $N(SiMe_2H)_2$). A general differential approach for the kinetic analysis of living polymerizations with fast propagation and comparatively slow initiation is presented. Time-resolved analysis of monomer conversion and molecular weights of the formed polymers allow the determination of the initiator efficiency throughout the whole reaction. Using this normalization method, rare earth metal-mediated vinylphosphonate GTP is shown to follow a Yasuda-type monometallic propagation mechanism, with an S_N2-type associative displacement of the polymer phosphonate ester by a monomer as the rate-determining step. The propagation rate of vinylphosphonate GTP is mainly determined by the activation entropy, i.e. the change of rotational and vibrational restrictions within the eight-membered metallacycle in the rate-determining step as a function of the steric demand of the metallacycle side chains and the steric crowding at the metal center.

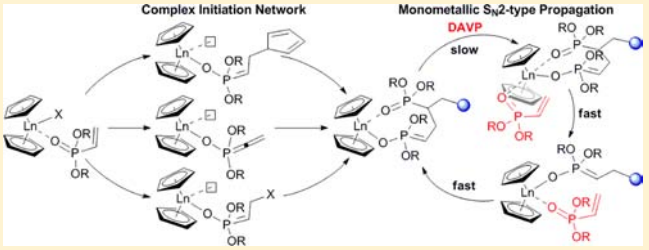

INTRODUCTION

Phosphorus-containing polymers, especially those comprising phosphonate moieties, have gained significant interest due to their potential utilization in a large variety of applications, ranging from polyelectrolytes in batteries and fuel cells over halogen-free flame retardants to diverse uses in the biomedical field.[1−10] However, a straightforward approach to these polymers *via* polymerization of vinylphosphonates has long been hard to establish, as radical and classical anionic synthesis routes often result in low yields of polymer with unsatisfying degrees of polymerization.[11] Recently, it could be shown that poly(vinylphosphonate)s with high molar mass and low polydispersity can be efficiently prepared in the presence of rare earth metal catalysts,[11−16] presumably following a group transfer polymerization (GTP) mechanism.[11]

Rare earth metal-mediated GTP (REM-GTP) of acrylic monomers was first reported by Yasuda et al.[17] in 1992 and is also referred to as coordinative-anionic or coordination-addition polymerization.[18] Over the past decades, intensive research has been carried out to optimize the reaction conditions and the initiator efficiency and to broaden the use of coordinative-anionic polymerizations for a variety of monomers, e.g. different (meth)acrylates and (meth)-acrylamides.[18−21] The initiation for this living-type of polymerization commonly occurs *via* 1,4-addition of a nucleophilic ligand from the metal complex to a coordinated monomer or, in the case of divalent lanthanide initiators, *via* redox initiation.[18,22] The propagation proceeds *via* repeated conjugate addition over an eight-membered ring intermediate (Scheme 1a),[18−21,23] which could be isolated and characterized by X-ray crystallography.[17,23] Hereby, the catalyst both stabilizes the anionic chain end and activates the coordinated monomer.[11,18] The coordination of the growing chain end at the catalyst suppresses side reactions and allows stereospecific polymerization as well as activity optimization by variation of both the metal center and the catalyst ligand sphere.[18−21] Besides this monometallic propagation, coordinative-anionic polymerizations may also follow a bimetallic mechanism, for which alternating one metal center activates the monomer, while the other stabilizes the growing chain end (e.g., for group 4 metal-mediated GTP, Scheme 1b).[24−28]

The mechanism taking place and the corresponding rate-determining step (RDS) are difficult to predict and were found

Received: May 13, 2013
Published: July 26, 2013

   dx.doi.org/10.1021/ja404457f | J. Am. Chem. Soc. 2013, 135, 13030−13040

Scheme 1. Proposed Monometallic (a) and Bimetallic (b) Propagation Mechanism for Coordinative-Anionic Polymerization of Michael Acceptor-Type Monomers[a]

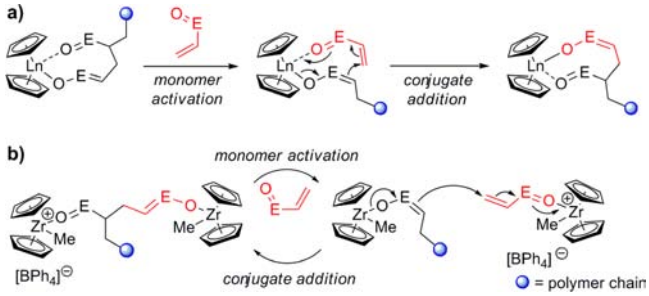

[a]E = C(OR), $C(NR_2)$, $P(OR)_2$.

Scheme 2. Proposed S_N1-Type (a) and S_N2-Type (b) Polymer Ester Cleavage from/Monomer Addition to the Metal Center for REM-GTP[a]

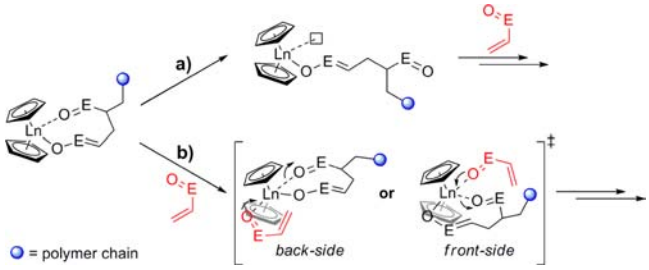

[a]E = C(OR), $C(NR_2)$, $P(OR)_2$.

to be strongly dependent on the ligand architecture, the metal center, and the used monomer.[18,25−27,29−36] The influence of mechanism and RDS on the stereoregularity of the polymerization and, *vice versa*, the mechanistic conclusions drawn from obtained microstructures have been controversially discussed.[20,28−30,33,36−40] Besides the actual conjugate addition, the RDS can be cleavage of the polymer ester group from the metal center (S_N1-type reaction, Scheme 2a) or an associative displacement of this ester group by a monomer (S_N2-type reaction, Scheme 2b).[20,25−30,36,37,40−42] The latter is both described in a back-side manner or *via* an attack at the same site relative to the leaving polymer ester group (front-side), *i.e. via* a chain retention or a chain migratory mechanism.[28−30,33,37−40,42] In the case of monometallic coordinative-anionic polymerization, depending on the evident RDS, the monomer addition will occur either alternating at both sites of the catalyst or predominantly at only one site *via* site-retention.[29,30,33,36−40,42]

Recent publications have shown that REM-GTP is not only applicable to common acrylic monomers, but as well to several other monomer classes, i.e. dialkyl vinylphosphonates (DAVP), 2-isopropylene-2-oxazoline and 2-vinylpyridine.[11−16,43,44] In previous work, we have shown that late lanthanide metallocenes are efficient initiators and highly active catalysts for DAVP polymerization.[14,16] Initial investigations have proven the livingness of polymerization and suggest a GTP mechanism taking place,[11,12,14] however, detailed mechanistic studies on both initiation and propagation of REM-GTP of vinylphosphonates have not yet been conducted.

In this article, we show that initiation of vinylphosphonate GTP follows a complex reaction network. We present a general procedure for kinetic analysis of living polymerizations with fast propagation and comparatively slow initiation. A detailed study of the influence of metal radii, steric demand of the monomers and reaction temperature on the polymerization rate gives insight into the mechanism of REM-GTP, both for vinylphosphonates in particular as well as for its general understanding.

RESULTS AND DISCUSSION

We previously reported on the use of tris(cyclopentadienyl)-lanthanide complexes (Cp_3Ln) for the polymerization of diethyl and diisopropyl vinylphosphonate (DEVP and DIVP, respectively).[14] Whereas the rate of initiation was found to be accelerated by both decreasing metal radius and increasing steric demand of the monomer, i.e. by higher steric crowding of the intermediate Cp_3Ln(DAVP), the propagation rate was enhanced by smaller metal radii and decreasing steric demand of the monomer, contradicting previous work on (meth)-acrylate rare earth metal-mediated GTP.[18−20,23,45] Within the frame of this previous work, we could not address the origin of this faster propagation for late lanthanides, i.e. for higher Lewis acidity and *higher* steric crowding of the active species, in combination with an increased activity for smaller monomers, *i.e. lower* steric crowding of the active species.

In earlier work, we applied bis(cyclopentadienyl)-chloro, -amide, and -methyl complexes ($[Cp_2LnCl]_2$, Cp_2Ln(bdsa)-(thf), and $[Cp_2YbMe]_2$, respectively; bdsa = bis(dimethylsilyl)-amide, $N(SiMe_2H)_2$) for vinylphosphonate polymerization.[11,12,46] For the chloro and amide catalysts, a distinct initiation period was evident. In accordance with their previous use for MMA polymerization, the observed initiator efficiencies were low; however, the activity is considerably higher for

Table 1. DEVP Polymerization Results for Previously Applied Cp_2LnX Catalysts[a]

catalyst	reaction time	conversion[b]/%	init. period[c]	M_n[d]/kDa	PDI (M_w/M_n)	I^*[d]/%	TOF[b]/I^*/h^{-1}	TOF/I^* (Cp_3Ln)[e]/h^{-1}
$[Cp_2HoCl]_2$	24 h	76	180 min	810	1.32	9.6	1100	8000
$[Cp_2YCl]_2$	6 h	70	100 min	740	1.31	9.3	3700	23000
$[Cp_2ErCl]_2$	6 h	79	100 min	780	1.35	10.0	2800	28000
$[Cp_2TmCl]_2$	3.5 h	86	90 min	990	1.29	8.5	5900	72000
$[Cp_2YbCl]_2$	3 h	81	90 min	890	1.36	9.8	8400	185000
$[Cp_2LuCl]_2$	1.5 h	93	7 min	780	1.34	11.7	20500	>265000
Cp_2Y(bdsa)(thf)	3 h	95	15 min	1040	1.27	9.0	7200	23000
Cp_2Lu(bdsa)(thf)	3 h	96	20 min	1350	1.20	7.0	21000	>265000
$[Cp_2YbMe]_2$	30 min	99	80 s	900	1.52	10.8	49000	185000

[a]Toluene, 30 °C, monomer-to-catalyst ratio 600:1. [b]Determined by ^{31}P NMR spectroscopic measurement, [c]Initiation period, reaction time until 3% conversion is reached, [d]Determined by GPC-MALS, $I^* = M_{th}/M_n$, $M_{th} = 600 \times M_{Mon} \times$ conversion, [e]normalized activity for corresponding Cp_3Ln.[14]

dx.doi.org/10.1021/ja404457f | J. Am. Chem. Soc. 2013, 135, 13030−13040

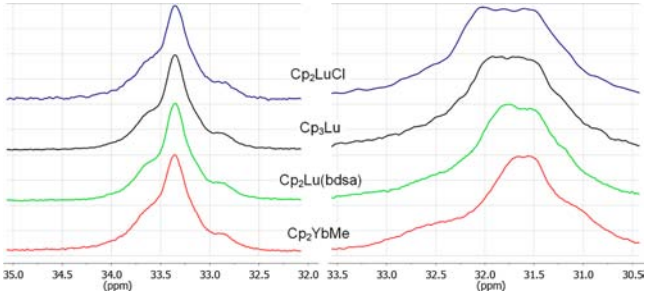

Figure 1. ^{31}P NMR spectra of PDEVP (left, in D_2O) and PDIVP (right, in $CDCl_3$) produced with different catalysts (from top to bottom: $[Cp_2LuCl]_2$ (blue), Cp_3Lu (black), $Cp_2Lu(bdsa)(thf)$, (green) and $[Cp_2YbMe]_2$ (red)). For all catalysts, polymers with (nearly) identical atactic polymer microstructure are obtained.

vinylphosphonate (Table 1) than for MMA polymerization (TOF = 7 h^{-1}).[18,47] According to our study on Cp_3Ln-initiated vinylphosphonate GTP, the normalized activity TOF/I*[14] was found to be strongly accelerated for later lanthanides, e.g. for $[Cp_2LnCl]_2$/DEVP from 1100 h^{-1} for Ho to 20500 h^{-1} for Lu (Table 1, entry 1–6).[14] At the same time, contradicting the polymerization with Cp_3Ln, the initiator efficiency was either unaffected by the metal size (Table 1) or found to decrease for smaller metal centers (see ref 11), depending on concentration and polymerization temperature. Hereby, all Cp_3Ln and Cp_2LnX complexes yielded polymers with the same (essentially) atactic polymer microstructure (Figure 1), indicating the active catalytic species consistently to be a Cp_2Ln unit. The normalized activity, however, was found to be strongly different for Cp_3Ln in comparison to that of $[Cp_2LnCl]_2$, $[Cp_2YbMe]_2$, and $Cp_2Ln(bdsa)(thf)$ (Table 1). In order to explain the observed differences between Cp_2LnX and Cp_3Ln complexes and the differences from (meth)acrylate polymerizations, we conducted detailed analyses of both initiation and propagation of vinylphosphonate GTP.

Initiation Mechanism. ESI MS analysis of vinylphosphonate oligomers produced with $[Cp_2YbMe]_2$ shows no apparent end group (Figure S1 in Supporting Information [SI]). As methanolic workup leads to chain termination by a proton, the exclusive observation of signals with $m/z = n \times M_{Mon} + M_{Na}$ is attributed to an initiation *via* deprotonation yielding CH_4 and an olefinic chain end. Similar to Cp_3Ln, for $[Cp_2LnCl]_2$, initiation was found to proceed *via* transfer of a cyclopentadienyl ligand to a coordinated monomer (Figure S2, S3 in SI).[14,48] These results clearly show that, depending on the ligand's basicity and nucleophilicity, initiation can generally either proceed *via* deprotonation of the acidic α-CH of the vinylphosphonate or *via* nucleophilic transfer (Scheme 3). This is in line with previous observations on classical anionic vinylphosphonate polymerizations.[11,49]

For the amide catalysts $Cp_2Ln(bdsa)(thf)$, on the other hand, two series of peaks were evident in the mass spectrometric end group analysis, one with a bdsa and one with a Cp end group (Figure 2). The ratio of these end groups

Scheme 3. Possible Initiation Reactions for Rare Earth Metal-Mediated Vinylphosphonate Polymerizations

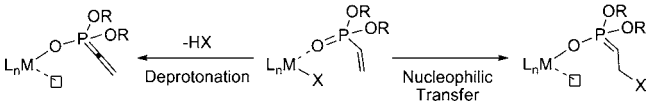

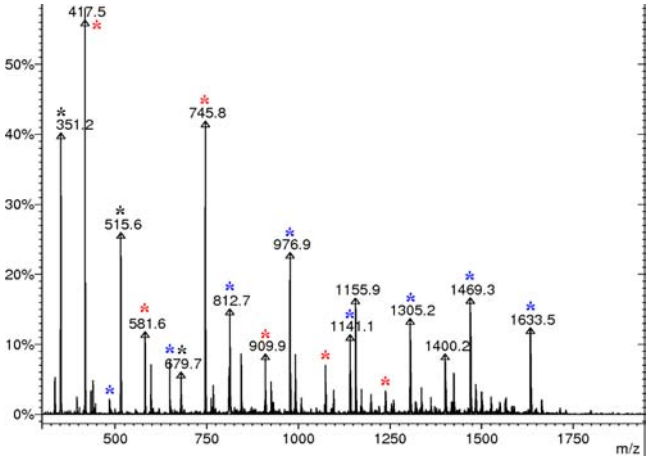

Figure 2. ESI MS spectrum of DEVP oligomers produced with $Cp_2Y(bdsa)(thf)$. Two major series of peaks are evident: $m/z = n \times M_{Mon} + 66 + M_{Na}$ (red), $m/z = n \times M_{Mon} + 133 + M_{Na}$ (blue); M_{Mon} = 164, end groups: $M_{Cp} + M_H$ = 66, $M_{bdsa} + M_H$ = 133. Peaks at m/z = 351, 515, and 679 are attributed to fragmentation (black).[48]

Scheme 4. Donor-Induced Ligand-Exchange Reaction Caused by Coordination of Phosphonates at Cp_2LnX Complexes for the Example DEEP

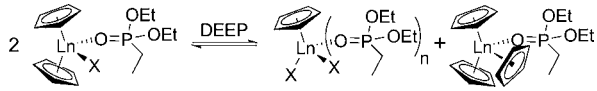

was found to be strongly dependent on the reaction conditions, and frequently, a peak series with olefinic chain ends was observed instead of bdsa end groups (Figures S4, S5 in SI). As in some cases, only olefinic chain ends were detected (Figure S5 in SI), this observation can be attributed to an elimination of the bdsa end group. Despite the simultaneous occurrence of two different initiation reactions, the obtained polymer shows a monomodal molecular weight distribution, indicating that both types of initiation produce the same active species.

To get deeper insight in the underlying initiation mechanism, an NMR spectroscopic study of phosphonate coordination at the used complexes was conducted. Diethyl ethylphosphonate (DEEP) was used due to its similar steric demand in comparison to DEVP and as it excludes both initiation and subsequent polymerization. Addition of varying amounts of DEEP (0.5, 1, 2, and 5 equiv with respect to the metal center, respectively) revealed a monomer (i.e., donor)-induced ligand exchange reaction forming $Cp_3Ln(DEEP)$ and $CpLnX_2(DEEP)_n$ in equilibrium with the adduct Cp_2LnX-(DEEP) (Scheme 4, Figure 3). Line broadening of the DEEP ^{1}H and ^{31}P NMR spectroscopic signals indicates a fast exchange (in the NMR time scale) of coordinated and free DEEP (Figure 3). Larger metal centers and higher phosphonate concentration accelerate this exchange reaction and shift the equilibrium to the $Cp_3Ln/CpLnX_2$ side.

To provide proof of the identity of the $Cp_3Ln(DEEP)$ adduct, the NMR samples of the corresponding Y complex were overlaid with pentane, yielding colorless crystals suitable for single-crystal X-ray crystallography (Figures 4 and S13 in SI). In attempts to crystallize a vinylphosphonate adduct, according to the prolonged initiation period, addition of 1 equiv of DEVP to a toluene solution of $[Cp_2LnCl]_2$ (Ln = Ho, Yb), subsequent overlaying with pentane, and cooling to −30 °C

dx.doi.org/10.1021/ja404457f | J. Am. Chem. Soc. 2013, 135, 13030−13040

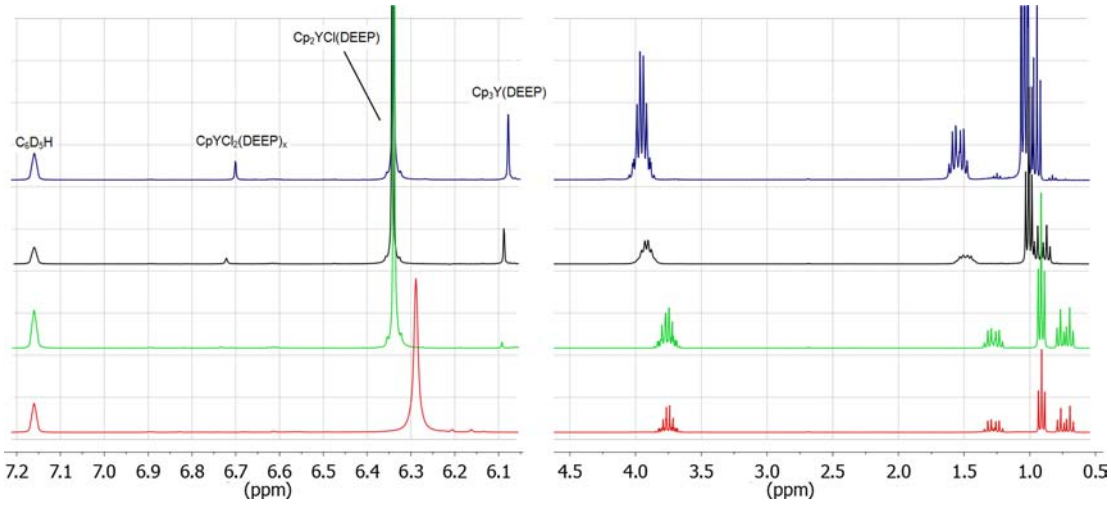

Figure 3. ^{1}H NMR spectra of DEEP coordination at the rare earth metal center for addition of 0.5 (red), 1 (green), 2 (black), and 5 equiv (blue) of DEEP (with respect to the metal center) to $[Cp_2YCl]_2$ in C_6D_6, respectively. A donor-induced ligand-exchange reaction forming $Cp_3Y(DEEP)$ and $CpYCl_2(DEEP)_n$ in equilibrium with the adduct $Cp_2YCl(DEEP)$ is evident. For addition of 2 equiv of DEEP, line broadening for the DEEP ^{1}H NMR spectroscopic signals shows an exchange of free and coordinated DEEP in the ^{1}H NMR time scale.

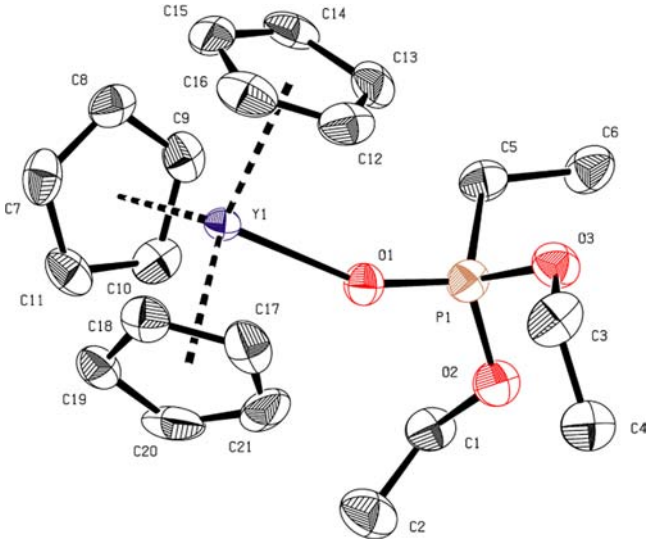

Figure 4. Crystal structure of the adduct $Cp_3Y(DEEP)$ (50% thermal ellipsoids; hydrogen atoms were omitted for clarity). Selected interatomic distances and bond angles: Y−O(1), 2.294 Å; P═O(1), 1.495 Å; Y−O(1)═P, 7.24°.

yielded the adduct $Cp_2LnCl(DEVP)$, as proven by X-ray crystallography. This way, we can provide first crystallographic proof of vinylphosphonate coordination at the active site *via* the oxygen of the phosphonate moiety (Figures 5 and S14, S15 in SI). Previously, this type of coordination was suggested by ^{1}H and ^{31}P NMR spectroscopies.[13,50] Importantly, the crystal structures show that the Michael system of the coordinated vinylphosphonate is retained in an S-cis conformation with a pronounced π-overlap (torsion angles O═P−C═C of −10.14 and 10.47°, Figures 5 and S14, S15 in SI), a key prerequisite for the polymerizability of a monomer by a repeated conjugate addition polymerization, i.e. a GTP.[11,18] When the isolated DEVP adducts are dissolved in toluene, vinylphosphonate oligomers are formed after a few hours at room temperature without the addition of further monomer. This inherent instability of the Cp_2LnCl (DEVP) adducts provides further evidence for the observed ligand-exchange reaction.

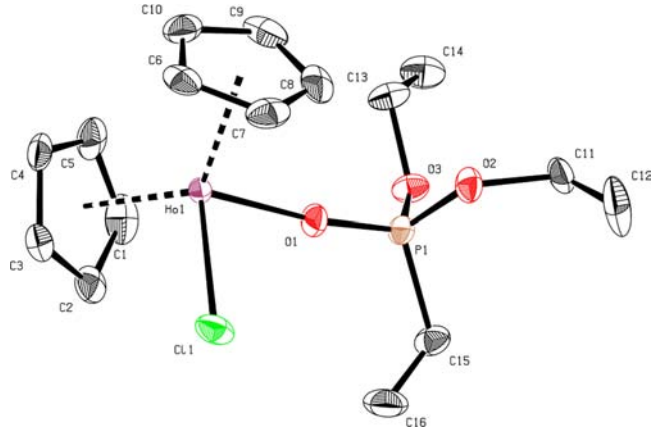

Figure 5. Crystal structure of the adduct $Cp_2HoCl(DEVP)$ (50% thermal ellipsoids; hydrogen atoms were omitted for clarity). Selected interatomic distances, bond angles, and torsion angles: Ho−Cl, 2.582 Å; Ho−O(1), 2.227 Å; P═O(1), 1.485 Å; P−C(15), 1.779 Å; C(15)═C(16), 1.314 Å; P═O(1)−Ho, 167.0°; O (1)═P−C(15)═C(16), −10.14°.

Different initiators, Cp_2LnX, were synthesized and tested for their vinylphosphonate polymerization behavior (Table 2). Except for the aryloxy-substituted complexes $Cp_2Ln(OAr)$-(thf), in all cases, the formation of $Cp_3Ln(DEEP)$ was observed. As previously shown, in the case of late lanthanides, $Cp_3Ln(DAVP)$ serves as an efficient initiator for DAVP polymerization.[14] If neither deprotonation of the acidic α-CH nor nucleophilic transfer is possible due to insufficient reactivity of the LnX bond (e.g., for X = Cl, O(Alk/Ar)), formed $Cp_3Ln(DAVP)$ will serve as the active initiating species (Scheme 5). This conclusion is corroborated by end group analysis of produced DEVP oligomers as well as by the inability of $Cp_2Ln(OAr)(thf)$ (which was found not to undergo a ligand-exchange reaction, but to decompose upon DEEP addition) and $Cp^*_2LuCl(thf)$ (for which formation of Cp^*_3Lu, and thus a ligand exchange is not possible[51]) to initiate polymerization (Table 2 and Figures S6−11 in SI).

Thiolato complexes $[Cp_2Ln(StBu)]_2$ were found to be well-suited for the initiation of vinylphosphonate GTP. However, for

dx.doi.org/10.1021/ja404457f | J. Am. Chem. Soc. 2013, 135, 13030−13040

Table 2. DEVP Polymerization Results for Cp_2LnX Catalysts[a]

catalyst	reaction time	conversion[b]/%	init. period[c]	M_n[d]/kDa	PDI (M_w/M_n)	I^*[d]/%	TOF[b]/I^* /h^{-1}	end group[e]	extent of ligand exchange[f]/%
$[Cp_2YCl]_2$	6 h	70	100 min	740	1.31	9.3	3700	Cp	15
$Cp_2Y(bdsa)(thf)$	3 h	95	15 min	1040	1.27	9.0	7200	Cp, bdsa (olefinic)[g]	3
$[Cp_2Y(OiPr)]_2$	30 h	26	2.5 h	1070	1.20	2.4	2000	Cp	<0.5 (10)[h]
$Cp_2Y(OAr)(thf)$	30 h	–	–	–	–	–	–	–	<0.5
$[Cp_2Y(StBu)]_2$	3 min	100	5 s	150	1.18	65	69000	StBu (olefinic)[g]	4
$Cp_2Y(CH_2TMS)(thf)$	40 min	88	5 min	510	1.45	17	10000	olefinic	5
$[Cp_2LuCl]_2$	1.5 h	93	7 min	780	1.34	11.7	20500	Cp	3
$Cp_2Lu(bdsa)(thf)$	3 h	96	20 min	1350	1.20	7.0	21000	Cp, bdsa (olefinic)[g]	1
$[Cp_2Lu(OiPr)]_2$	30 h	52	9 h	1270	1.18	4.0	600	Cp	<0.5 (<1)[h]
$Cp_2Lu(OAr)(thf)$	30 h	<1	–	–	–	–	–	–	<0.5
$[Cp_2Lu(StBu)]_2$	1.5 min	100	15 s	210	1.27	47	220000	StBu (olefinic)[g]	2
$Cp_2Lu(CH_2TMS)(thf)$	30 min	92	5 min	1130	1.38	8.0	39000	olefinic	1

[a]Toluene, 30 °C, monomer-to-catalyst ratio 600:1. [b]Determined by ^{31}P NMR spectroscopic measurement. [c]Initiation period, reaction time until 3% conversion is reached. [d]Determined by GPC-MALS, $I^* = M_{th}/M_n$, $M_{th} = 600 \times M_{Mon} \times$ conversion. [e]Determined by ESI MS. [f]Conversion of Cp_2LnX for addition of 5 equiv of DEEP, determined from ^1H NMR spectroscopic signals of Cp_2LnX(DEEP) and Cp_3Ln(DEEP). [g]Olefinic chain ends formed by end group elimination. [h]Number in brackets: extent of dimer opening for addition of 5 equiv of DEEP, determined from ^1H NMR spectroscopic signals of $Cp_2Ln(OiPr)$(DEEP) and DEEP.

Scheme 5. Initiation of Vinylphosphonate GTP Using Unbridged Rare Earth Metallocenes (Cp_2LnX) *via* Deprotonation of the Acidic α-CH, Nucleophilic Transfer of X, or a Monomer-Induced Ligand-Exchange Reaction Forming Cp_3Ln(DAVP)

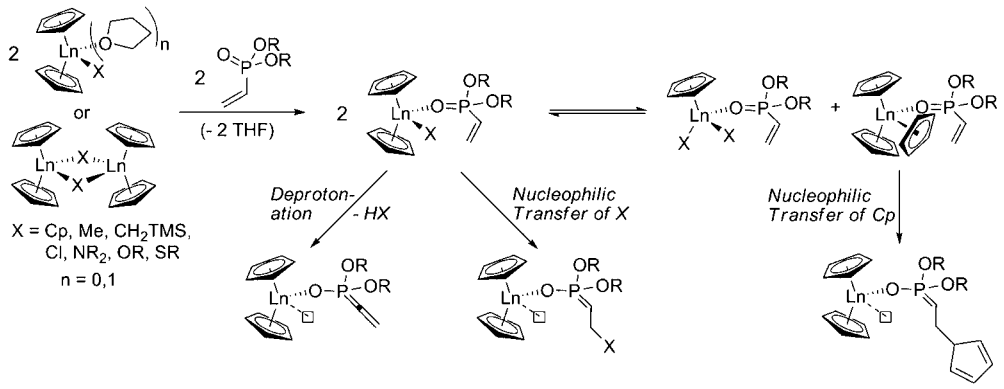

the observed fast transfer of thiolates to a coordinated monomer, the opening of dimers by coordination of a vinylphosphonate becomes rate-limiting (Scheme 5), as underlined by the lengthened initiation period and lower I^* of the more stable $[Cp_2Lu(StBu)]_2$ dimer in comparison to its Y analogue (Table 2, entries 5 and 11). For the more stable alkoxy dimers (e.g., $[Cp_2Ln(OiPr)]_2$), this limitation was observed also for the stronger coordinating vinylphosphonates as an incomplete reaction with DEEP to form $Cp_2Ln(OiPr)$(DEEP) (Table 2, entries 3 and 9)). Similar to bdsa, StBu end groups were found to be prone to elimination (Figures S8, S9 in SI). Steric repulsion is a major driving force of the elimination reaction, as larger monomers, e.g. DIVP, were found to facilitate this reaction, i.e. StBu end groups could not be found in ESI MS analysis of produced PDIVP oligomers (Figure S12 in SI). According to $[Cp_2YbMe]_2$, ESI MS analysis of DEVP oligomers produced with strongly basic CH_2TMS initiators revealed an initiation by deprotonation of the acidic α-CH of the vinylphosphonate. The low initiator efficiencies of both Me and CH_2TMS initiators (Tables 1 and 2) show that deprotonation of α-acidic monomers is a slow and thus unsuitable form of initiation for REM-GTP.

The above results show that the initiation of vinylphosphonate REM-GTP with unbridged rare earth metallocenes (Cp_2LnX) follows a complex reaction pathway (Scheme 5). Depending on the nature of X, initiation can either proceed *via* an abstraction of the acidic α-CH of the vinylphosphonate (e.g., for X = Me, CH_2TMS), *via* nucleophilic transfer of X to a coordinated momoner (e.g., for X = Cp, SR) or *via* a monomer (i.e., donor)-induced ligand-exchange reaction forming Cp_3Ln in equilibrium (e.g., for X = Cl, OR), which serves as the active initiating species. Each of the reaction steps (Scheme 5) can be rate-limiting, and different initiations may also occur simultaneously (e.g., for X = $N(SiMe_2H)_2$). Only nucleophilic transfer was found to ensure a homogeneous initiation of REM-GTP of vinylphosphonates, as the occurring initiation by deprotonation using the common strongly basic methyl, CH_2TMS, or hydride initiators[18−21] is rather slow.

Propagation Mechanism. The investigations on the initiation mechanism revealed that Cp_2LnX-initiated vinylphosphonate polymerizations are generally mediated by a Cp_2Ln unit. Nevertheless, the observed normalized activities TOF/I^* of different bis(cyclopentadienyl) complexes with identical metal centers are not the same (Tables 1 and 2). For

dx.doi.org/10.1021/ja404457f | J. Am. Chem. Soc. 2013, 135, 13030−13040

ideal living polymerizations, i.e. living polymerizations for which the initiation rate is considerably faster than the propagation rate, I^* is mainly determined by an initial initiator deactivation and therefore does not change during the course of polymerization. REM-GTP of vinylphosphonates is very fast and therefore primarily limited by an inefficient initiation reaction. Thus, the initiator efficiency I^* is significantly increasing during polymerization. Consequently, for a proper comparison of the catalytic activity, I^* has to be determined throughout the whole reaction. Better normalization results are yielded, if the initiator efficiency at the maximum rate of monomer conversion I^*_t is used instead of this efficiency at the end of the reaction (Figure 6).

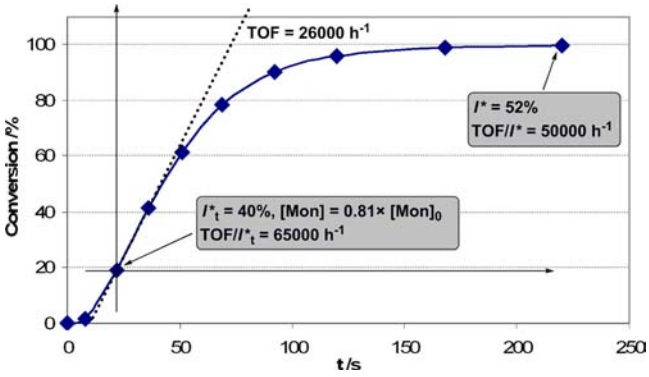

Figure 6. Conversion-reaction time plot for polymerization of DEVP, change of I^*_t during the reaction, and corresponding normalized TOFs (8.6 mg $[Cp_2Y(StBu)]_2$, 7.5 vol % DEVP in toluene (20 mL), 30 °C).

For the very fast polymerization of DEVP, the maximum rate is typically observed for a conversion of approximately 15−40% (Figure 6). Thus, temperature (it is not possible to completely remove the reaction heat from the system) and viscosity effects cannot be entirely excluded, especially for high monomer concentrations. As GTP is sensitive to protic impurities and since GPC analysis needs to be performed with the aliquots taken in order to determine I^*_t, there is also a lower concentration limit for reliable kinetic analysis. In our study, we found that 2.5−10 vol % monomer concentrations in toluene are ideal.

The general rate law for catalyzed polymerizations reads

$$r = k \times [\mathrm{Cat}]^m \times [\mathrm{Mon}]^n \quad (1)$$

For a meaningful kinetic analysis, we use the maximum rate of conversion, the present active catalyst concentration [Cat*], and the residual monomer concentration [Mon]. In accordance with a living-type polymerization, we calculate these concentrations following

$$[\mathrm{Cat}^*] = [\mathrm{Cat}]_0 \times I^*_t \quad (2)$$

and

$$[\mathrm{Mon}] = [\mathrm{Mon}]_0 \times (1 - C) \quad (3)$$

with the overall catalyst concentration $[\mathrm{Cat}]_0$, the initial monomer concentration $[\mathrm{Mon}]_0$, the conversion C, and

$$I^*_t = M_{\mathrm{Mon}} \times ([\mathrm{Mon}]_0/[\mathrm{Cat}]_0) \times C/M_n \quad (4)$$

with the monomer molar mass M_{Mon} and the number-averaged molecular weight M_n at the given reaction time t as determined *via* absolute analysis using GPC-MALS. This normalization with the initiator efficiency I^*_t addresses both inefficient initiation and catalyst deactivation due to (protic) impurities.

As the initiator efficiency depends on concentration and monomer-to-catalyst ratio, the active catalyst concentration cannot be exactly predicted. Thus, for the determination of the reaction orders, first, the initial monomer concentration is kept constant to determine the order in catalyst m. For different concentrations of the same catalyst at otherwise identical reaction conditions, the maximum rate is consistently reached at similar conversion. Therefore, the residual monomer concentration is also assumed to be constant, and $\ln(r)$ is plotted against $\ln([\mathrm{Cat}^*])$ yielding a reaction order of $m = 1$ for every evaluated catalyst (Figures 7 and S16 and Tables S1 and S2 in SI). Consequently, rare earth metal-mediated vinylphosphonate GTP follows a monometallic propagation according to the mechanism previously shown for (meth)acrylic monomers (Scheme 1a).

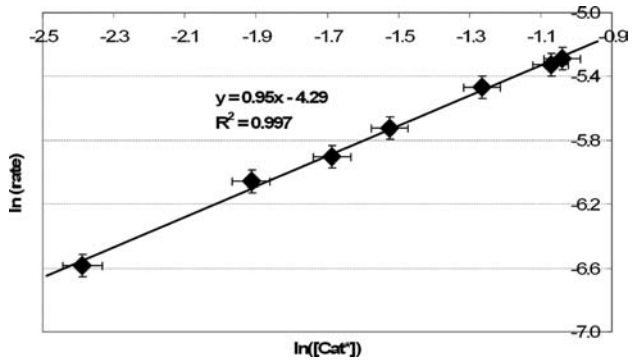

Figure 7. Determination of catalyst order (Cp_3Tm, 5 vol % DEVP in toluene, 30 °C).

In order to verify the corresponding RDS, the monomer order n is determined by the following:

$$r/[\mathrm{Cat}^*] = k \times [\mathrm{Mon}]^n \quad (5)$$

by plotting $\ln(r/[\mathrm{Cat}^*])$ against $\ln([\mathrm{Mon}])$.

The viscosity of the reaction mixture is strongly affected by the initial monomer concentration, thus making a reliable determination of the monomer reaction order difficult. Only catalysts with high initiator efficiency, I^*_t, allow kinetic analysis of the monomer order, as they both yield lower-molecular weight polymers and exhibit their maximum rate for rather low conversions (below 30%). Moreover, an initial heterogeneous polymerization is observed for fast initiating complexes with poor solubility in toluene, such as Cp_3Ln. Accordingly, Cp_3Tm allows determination of the catalyst order for DEVP polymerization, as it dissolves completely during an initiation period of approximately one minute, providing initiator efficiencies I^*_t of 13−21% (Figure 7 and Table S1 in SI). However, for these low initiator efficiencies, a reliable determination of monomer orders is not possible. In addition, catalyst orders for DIVP polymerization may not be obtained using Cp_3Ln due to an occurring initial heterogeneous polymerization.

For this purpose, a better soluble complex with higher initiator efficiency is necessary. $[Cp_2Y(StBu)]_2$ was used as it dissolves instantly upon monomer addition and reaches initiator efficiencies I^*_t of 35−54% and 57−86% in the case of DEVP and DIVP polymerization, respectively (Tables S2−S5 in SI). Using this thiolato yttrocene, the order in catalyst for DIVP polymerization could be determined as $m = 1$, showing

dx.doi.org/10.1021/ja404457f | J. Am. Chem. Soc. 2013, 135, 13030−13040

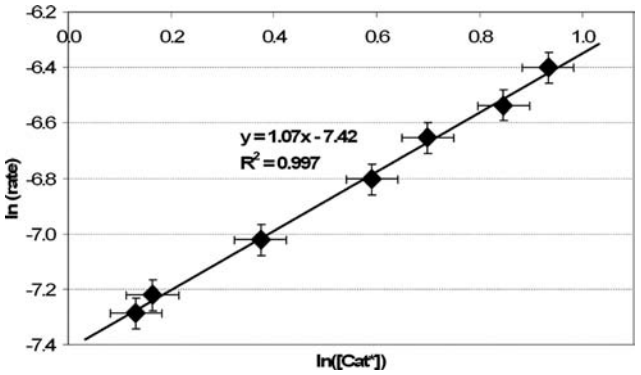

Figure 8. Determination of catalyst order ($[Cp_2Y(StBu)]_2$, 12.5 vol % DIVP in toluene, 30 °C.

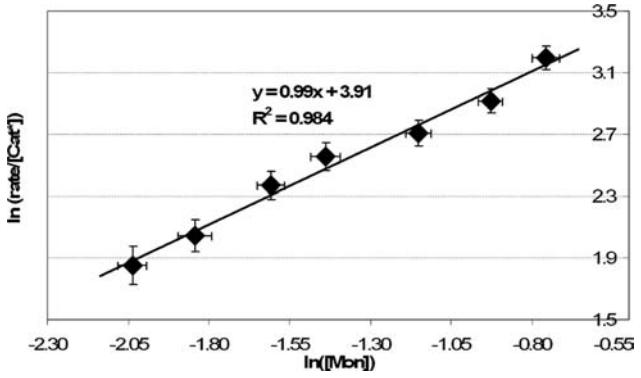

Figure 9. Determination of monomer order ($[Cp_2Y(StBu)]_2$, 2.5–10 vol % DEVP in toluene, 30 °C).

that increase of the monomer steric demand does not lead to a change of the propagation mechanism (Figure 8, Table S3 in SI). Determination of the monomer order according to equation (5) yields $n = 1$ for polymerization of both DEVP and DIVP (Figures 9, S17, Tables S4, S5 in SI). These results show that rare earth metal-mediated vinylphosphonate GTP follows a monometallic Yasuda-type polymerization mechanism, with an S_N2-type associative displacement of the polymer phosphonate ester by a monomer as the RDS as depicted in Scheme 2b. Whether the addition of vinylphosphonate occurs *via* a back-side or front-side attack, *i.e. via* chain-retention or chain migratory mechanism, may not be verified this way. For this purpose, studies on the stereospecifity of C_S- or C_1-symmetric catalysts and/or theoretical calculations need to be performed. Such studies are currently underway in our laboratories.

Still, these results provide no explanation of the origin of the influence of metal radii and steric demand of monomers on the catalytic activity. For this purpose, temperature-dependent kinetic analysis was performed to determine activation enthalpies $\Delta H^{\ddagger}$ and entropies $\Delta S^{\ddagger}$ according to the Eyring equation

$$\ln(k/T) = -\Delta H^{\ddagger}/R \times 1/T + \Delta S^{\ddagger}/R + \ln(k_B/h) \qquad (6)$$

with the rate constant k, the temperature T, the gas constant R, the Boltzmann constant k_B, and the Planck constant h. Plotting $\ln(k/T)$ against $1/T$ yields the activation enthalpy and entropy of the RDS (Figure 10).

These experiments were performed for the metal centers Lu, Tm, Y, and Tb (in order of increasing metal ionic radius[52]) as

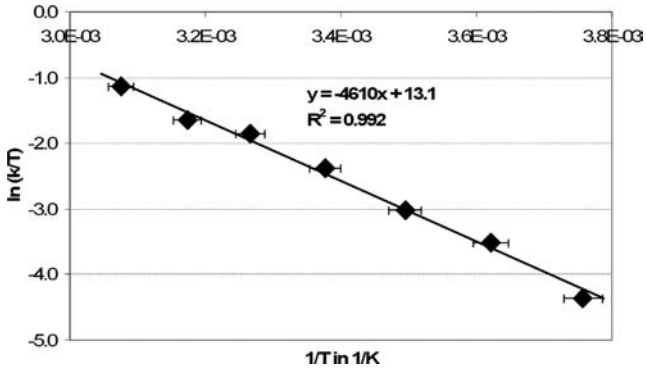

Figure 10. Eyring plot for $[Cp_2Y(StBu)]_2$-initiated DEVP (10 vol %) polymerization in toluene (−7 to 52 °C, $\Delta H^{\ddagger}$ = 38.3 kJ mol^{-1}, $\Delta S^{\ddagger}$ = −88.6 J (mol K)$^{-1}$).

Table 3. Activation Enthalpy $\Delta H^{\ddagger}$ and Entropy $\Delta S^{\ddagger}$ Dependence on Ionic Radius and Monomer Steric Demand

		DEVP		DIVP	
metal center	radius/ pm[a]	$\Delta H^{\ddagger}$/ kJ mol^{-1}	$\Delta S^{\ddagger}$/ J (K mol)$^{-1}$	$\Delta H^{\ddagger}$/ kJ mol^{-1}	$\Delta S^{\ddagger}$/ (J K mol)$^{-1}$
Tb	106.3	38.5	−102	41.3	−124
Y	104.0	38.3	−88.6	40.7	−112
Tm	102.0	39.1	−82.8	–	–
Lu	100.1	38.7	−73.6	42.0	−99.1

[a] Ln^{3+} ionic radius.[52]

well as for the monomers DEVP and DIVP (Table 3 and Figures S6–S12 in SI, Figures 10 and S18–S23 in SI). Contradicting the reactivity order of different rare earth metals for MMA polymerization previously reported by Yasuda et al. (Sm > Y > Yb > Lu),[23] vinylphosphonate GTP is accelerated by a decreasing ionic radius of the metal center (see also ref 14). Surprisingly, for both monomers, $\Delta H^{\ddagger}$ was found not to be affected by the metal ionic radius (within the limits of experimental accuracy of ∼1–2 kJ mol^{-1}). Thus, enthalpic effects, e.g. the Ln–(O═P) bond strength as a function of the Lewis acidity and the metallacycle ring strain as a function of the radius of the metal center, therefore do not determine the activity of different rare earth metals for vinylphosphonate GTP. In fact, different activation barriers $\Delta G^{\ddagger}$ were found to be a result of a change of $-T\Delta S^{\ddagger}$, which was found to decrease linearly with decreasing metal ionic radius (Table 3, Figure 11).

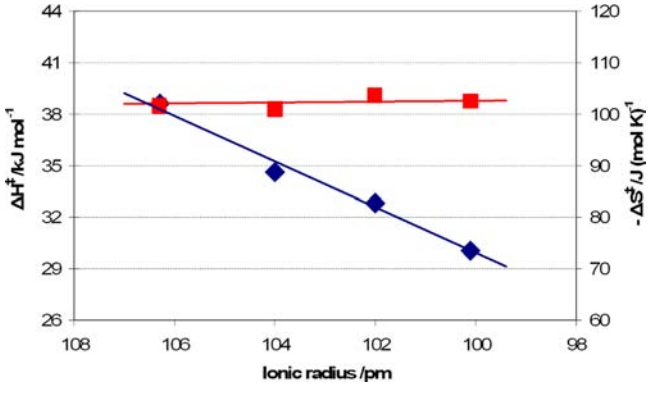

Figure 11. Activation enthalpy (red squares) and entropy (blue diamonds) for DEVP polymerization using Cp_2LnX catalysts in dependence of the metal ionic radius.

Scheme 6. Elemental Steps of Rare Earth-Mediated GTP of Vinylphosphonates[a]

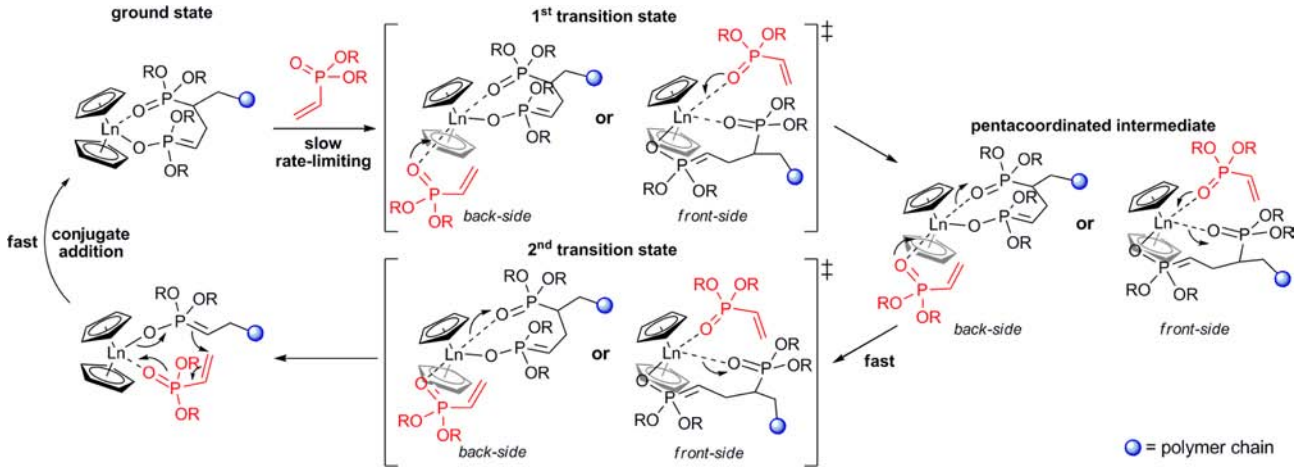

[a]The rate-limiting step is an S_N2-type associative displacement of the polymer phosphonate ester by a vinylphosphonate monomer, presumably *via* a pentacoordinated intermediate.

An increase of monomer steric demand leads to an increase of both $\Delta H^{\ddagger}$ and $-T\Delta S^{\ddagger}$ (Table 3). Hereby, at room temperature, the change of $\Delta S^{\ddagger}$ has a larger effect on the propagation rate ($\Delta\Delta H^{\ddagger} \approx 3$ kJ mol^{-1}, $-T\Delta\Delta S^{\ddagger} \approx 7$ kJ mol^{-1} for DEVP vs DIVP).

Importantly, a recent study on statistical copolymerization of different DAVPs revealed that the rate of vinylphosphonate GTP is mainly determined by the steric demand of the growing chain end, not by the added monomer.[16] Taking these considerations into account, the following mechanistic conclusions on rare earth metal-mediated GTP of vinylphosphonates can be drawn:

(1) The steric demand of the incoming monomer only shows minor influence on the propagation rate. Ziegler et al.[28] have shown coordinative-anionic polymerization of MA to proceed *via* a pentacoordinated intermediate with its formation by coordination of MA as the RDS. In the corresponding transition state, the metal−(O═C) bond to the incoming monomer is much longer than the metal−(O═C) bond to the polymer ester. In the present case, assuming REM-GTP of DAVP also proceeds over a pentacoordinated intermediate, the longer Ln−(O═P) bond in the corresponding transition state leads to a relatively small steric demand of the added vinylphosphonate in comparison to the growing chain end. The resulting minor effect of the steric demand of the added monomer on the propagation rate is in accordance with our observations (*vide supra*), thus providing initial evidence for the associative displacement to proceed over two transition states *via* a pentacoordinated intermediate (Scheme 6).

(2) Smaller metal centers destabilize the propagation ground state by a more confined arrangement of the eight-membered metallacycle according to the higher steric constraints caused by shorter Ln−Cp, Ln−(O−P) and Ln−(O═P) bonds. Contradicting to our expectation, the destabilization of the ground state is not of enthalpic (i.e., ring strain or the Ln−(O═P) bond strength), but of entropic nature (i.e., rotational and vibrational limitations in the eight-membered metallacycle). In the transition state, the Ln−(O═P) polymer phosphonate ester bond is lengthened, thus compensating part of the steric stress induced by the coordination of a vinylphosphonate monomer. This effect is larger for a stronger destabilization of the ground state, i.e. for smaller metal centers. Accordingly, we also expect an acceleration of vinylphosphonate REM-GTP by the introduction of sterically more demanding ligand systems (e.g., Cp^*_2 instead of Cp_2). Such studies are currently underway in our laboratories

(3) Higher steric demand of the growing polymer chain end (i.e., sterically more demanding side chains) leads to a relative destabilization of the transition state by both enthalpic and entropic effects, with the latter having the larger impact on the activation barrier. In comparison to the propagation ground state, the incoming monomer increases the steric crowding at the metal center (Scheme 6), leading to higher steric constraints within the eight-membered metallacycle, however, with the actual monomer size playing only a minor role (*vide supra*). In contrast, larger metallacycle side chains induce a stronger increase of rotational and vibrational restrictions in the RDS, thus destabilizing the transition state.

In summary, the propagation rate of vinylphosphonate GTP is mainly determined by the change of rotational and vibrational restrictions within the eight-membered metallacycle in the RDS as a function of the steric demand of the metallacycle side chains and the steric crowding at the metal center. In previous mechanistic studies on coordinative-anionic polymerization of (meth)acrylates, entropic effects have been largely disregarded,[27,28,32,36−40] even if Eyring plots were conducted.[37] In contrast to (meth)acrylates, the constitution of DAVP is tetrahedral and DAVPs are sterically more demanding. Therefore, rotational limitations and thus entropic effects are believed to have a stronger effect on DAVP than for (meth)acrylate GTP. However, taking into account the drastic effect of the metal radius and the monomer size on the activation entropy for vinylphosphonate GTP, also for (meth)acrylic monomers, experimental studies on activation entropies and theoretical studies on the free energy surface with a separate investigation of enthalpic and entropic effects may provide useful insight into the mechanism of monometallic rare earth metal/group 4 metallocenium cation-mediated GTP.

In case of coordinative-anionic polymerizations, it is well-established that the metal center has to remain easily accessible in order to ensure high activities. The current study and the present activity trend for vinylphosphonate GTP (smaller metal centers yield highly active catalysts) questions the general applicability of this concept. This conclusion is in line with

dx.doi.org/10.1021/ja404457f | J. Am. Chem. Soc. 2013, 135, 13030−13040

previous observations by Chen et al.,[40] which have found that an increase of steric crowding at the active site not only yields higher stereospecifity and a suppression of side reactions but also an acceleration of the propagation. Hence, in order to obtain high activity, the steric crowding of the catalyst needs to be well-adjusted: high enough to ensure sufficient destabilization of the eight-membered metallacycle ground state and to prohibit unfavored side reactions (e.g., site epimerization) and small enough to still facilitate an S_N2-type associative displacement of the polymer ester by an incoming monomer.

CONCLUSION

In this contribution, the first detailed mechanistic studies on both initiation and propagation of rare earth metal-mediated GTP of vinylphosphonates have been presented. During the course of our study, we were able to isolate the DEVP adducts, Cp_2LnCl (DEVP), providing the first X-ray crystallographic proof for vinylphosphonate coordination at the active site *via* the oxygen of the phosphonate moiety, and thus further supporting the hypothesis of GTP mechanism taking place. We have shown that the reactive α-CH and the use of unbridged rare earth metallocenes lead to a complex initiation network for vinylphosphonate GTP. Depending on the nature of the initiating ligand, initiation can either proceed *via* abstraction of the acidic α-CH of the vinylphosphonate, *via* transfer of a nucleophilic ligand to a coordinated monomer, or *via* a monomer (i.e., donor)-induced ligand-exchange reaction forming Cp_3Ln in equilibrium. We found the applied initiators, especially traditionally used strongly basic methyl, CH_2TMS, or hydride initiators, to suffer from different limitations, thus restricting their efficient use to selected monomers only. Therefore, rare earth metal-based GTP catalysts still require further development of versatile initiating ligands for an efficient application to a variety of monomers.

A detailed kinetic analysis of DAVP REM-GTP has been complicated by a very fast polymerization reaction in combination with a comparatively slow initiation. Thus, the overall reaction rate is influenced by both initiation and propagation. In this contribution, we have shown a general differential approach to separately analyze the propagation reaction for such living polymerizations. Time-resolved analysis of monomer conversion and molecular weights of the formed polymers allows the determination of the initiator efficiency throughout the whole reaction. Using this normalization method, rare earth metal-mediated GTP was shown to follow a monometallic Yasuda-type polymerization mechanism, with an S_N2-type associative displacement of the polymer phosphonate ester by a monomer as the RDS. The activation entropy $\Delta S^{\ddagger}$ of the RDS is strongly affected by the metal radius and the monomer size, whereas these parameters show only minor influence on the activation enthalpy $\Delta H^{\ddagger}$. As the steric demand of the added monomer shows only a minor influence on the propagation rate, the associative displacement is very likely to proceed over two transition states *via* a pentacoordinated intermediate. In order to support the mechanistic conclusions drawn in this contribution, further studies with a modified ligand architecture (especially C_1- and C_s-symmetric complexes) as well as theoretical calculations are currently underway.

EXPERIMENTAL SECTION

General. All reactions were carried out under argon atmosphere using standard Schlenk or glovebox techniques. All glassware was heat dried under vacuum prior to use. Unless otherwise stated, all chemicals were purchased from Sigma-Aldrich, Acros Organics, or ABCR and used as received. Toluene, thf and pentane were dried using an MBraun SPS-800 solvent purification system. Hexane, isopropanol, *tert*-butylthiol and DEEP were dried over 3 Å molecular sieves. Cp_3Ln,[53] $[Cp_2LnCl]_2$,[54] $[Cp_2YbMe]_2$,[55] $Cp^*_2LuCl(thf)$,[56] NaCp,[57] Li(bdsa),[58] the precursor complexes $Ln(bdsa)_3(thf)_2$ and $Ln(CH_2TMS)_3(thf)_2$,[58,59] as well as the monomers DEVP and DIVP[49] were prepared according to literature procedures. Monomers were dried over calcium hydride and distilled prior to use.

NMR spectra were recorded on a Bruker AV-300 or AV-500C spectrometer. ^{1}H-, ^{13}C-, and ^{29}Si NMR spectroscopic chemical shifts δ are reported in ppm relative to tetramethylsilane. δ (^{1}H) is calibrated to the residual proton signal, δ (^{13}C) to the carbon signal, and δ (^{29}Si) to the deuterium signal of the solvent. ^{31}P NMR spectroscopic chemical shifts are reported in ppm relative to and calibrated to 85% aqueous H_3PO_4. Deuterated solvents were obtained from Deutero or Eurisotop and dried over 3 Å molecular sieves. Elemental analyses were measured at the Laboratory for Microanalytics at the Institute of Inorganic Chemistry at the Technische Universität München. ESI MS analytical measurements were performed with methanol solutions on a Varian 500-MS spectrometer, using 70 keV in the positive ionization mode. IR spectra were recorded under argon atmosphere on a Bruker Vertex 70 spectrometer with a Bruker Platinum ATR setup and the integrated MCT detector. Samples were applied as thf solution or Et_2O suspension and measured after evaporation of the solvent. GPC was carried out on a Varian LC-920 equipped with two analytical PL Polargel M columns. As eluent, a mixture of 50% thf, 50% water, and 9 g L^{-1} tetrabutylammonium bromide (TBAB) was used in the case of PDEVP; for PDIVP analysis, the eluent was thf with 6 g L^{-1} TBAB. Absolute molecular weights have been determined online by multiangle light-scattering (MALS) analysis using a Wyatt Dawn Heleos II in combination with a Wyatt Optilab rEX as concentration source.

Complex Synthesis. *General Procedure for Synthesis of $Cp_2Ln(bdsa)(thf)$.* Two equivalents of freshly distilled cyclopentadiene are added to a toluene solution of 1equiv of $Ln(bdsa)_3(thf)_2$ (~0.25 M). The resulting solution is stirred overnight at 110 °C in a pressure Schlenk vessel, the solvent and formed 1,1,3,3-tetramethyldisilazane are removed *in vacuo*, and the resulting solid is recrystallized from toluene at −35 °C.

General Procedure for Synthesis of $Cp_2Ln(CH_2TMS)(thf)$. Two equivalents of freshly distilled cyclopentadiene are added to a toluene solution of 1 equiv of $Ln(CH_2TMS)_3(thf)_2$ (~0.25 M). The resulting solution is stirred overnight at rt, the solvent and formed tetramethylsilane are removed *in vacuo*, and the resulting solid is recrystallized from toluene/hexane at −35 °C.

General Procedure for Synthesis of Cp_2LnX. One equivalent of a stem solution of XH in toluene (~5 wt %) is added dropwise to a toluene solution of 1 equiv of $Cp_2Ln(bdsa)(thf)$ (~0.1 M). The resulting mixture is stirred overnight at rt, and the solvent and formed 1,1,3,3-tetramethyldisilazane are removed *in vacuo*, yielding pure product in quantitative yield.

For characterization of the synthesized organometallic compounds, see the Supporting Information.

Single-Crystal X-ray Structure Determinations. *$Cp_3Y(DEEP)$:* crystal data: formula $C_{21}H_{30}O_3PY$; M_r = 450.33; crystal color and shape: colorless fragment, crystal dimensions: 0.18 mm × 0.41 mm × 0.51 mm; crystal system: monoclinic; space group: $P2_1/n$ (no. 14); a = 11.5091 Å (4), b = 8.2872 (3) Å, c = 22.6167 (8) Å, β = 101.516 (2)°; V = 2113.72 (13) Å^3 ; Z = 4; μ (Mo Kα) = 2.851 mm^{-1}; ρ_{calcd} = 1.415 g cm^{-3}; θ-range = 1.84−25.36°; data collected: 75310; independent data [$I_o > 2\sigma(I_o)$/all data/R_{int}]: 3531/3849/0.041; data/restraints/parameter: 3849/0/238; $R1[I_o > 2\sigma(I_o)$/all data]: 0.0446/0.0485; $wR2[I_o > 2\sigma(I_o)$/all data]: 0.1182/0.1211; GOF = 1.074; $\Delta\rho_{max/min}$: 2.98/−0.86 eÅ^{-3}.

$Cp_2HoCl(DEVP)$: crystal data: formula $C_{16}H_{23}ClHoO_3P$; M_r = 494.69; crystal color and shape: colorless fragment; crystal dimensions: 0.18 mm × 0.51 mm × 0.64 mm; crystal system: orthorhombic; space group: $Pna2_1$ (no. 33); a = 20.7465 (6) Å, b = 11.7265 (4) Å, c =

7.8125 (3) Å; V = 1900.66 (11) Å^3 ; Z = 4; μ (Mo Kα) = 4.395 mm^{-1}; ρ_{calcd} = 1.729 g cm^{-3}; θ-range = 1.96−25.42°; data collected: 51428; independent data [$I_o > 2\sigma(I_o)$/all data/R_{int}]: 3484/3487/0.044; data/restraints/parameter: 3487/1/202; $R1[I_o > 2\sigma(I_o)$/all data]: 0.0144/0.0145; $wR2[I_o > 2\sigma(I_o)$/all data]: 0.0369/0.0369; GOF=1.197; $\Delta\rho_{max/min}$: 0.91/−0.73 eÅ^{-3}.

$Cp_2YbCl(DEVP)$: crystal data: formula $C_{16}H_{23}ClO_3PYb$; M_r = 502.80; crystal color and shape: colorless fragment, crystal dimensions: 0.18 mm × 0.51 mm × 0.53 mm; crystal system: orthorhombic; space group: $Pna2_1$ (no. 33); a = 20.7504 (7) Å, b = 11.7361 (4) Å, c = 7.8075 (3) Å; V = 1901.35 (12) Å^3 ; Z = 4; μ (Mo Kα) = 5.151 mm^{-1}; ρ_{calcd} = 1.757 g cm^{-3}; θ-range =1.96−25.36°; data collected: 46215; independent data [$I_o > 2\sigma(I_o)$/all data/R_{int}]: 3449/3461/0.053; data/restraints/parameter: 3461/1/201; $R1[I_o > 2\sigma(I_o)$/all data]: 0.0142/0.0143; $wR2[I_o > 2\sigma(I_o)$/all data]: 0.0373/0.0374; GOF = 1.088; $\Delta\rho_{max/min}$: 0.70/−0.55 eÅ^{-3}.

For detailed information, see Supporting Information. CCDC 930675 (**Cp_3Y(DEEP)**), CCDC 930674 (**Cp_2HoCl(DEVP)**), and CCDC 930673 (**Cp_2YbCl(DEVP)**) contain the supplementary crystallographic data for this compound. These data can be obtained free of charge from The Cambridge Crystallographic Data Centre *via* www.ccdc.cam.ac.uk/data_request/cif or *via* https://www.ccdc.cam.ac.uk/services/structure_deposit/.

Oligomerization. Five equivalents of DEVP are added to 1 equiv of catalyst in toluene. The resulting mixture is stirred for 2 h at room temperature and quenched by addition of MeOH or acidified (37 wt % HCl_{aq}) MeOH. Volatiles were removed under reduced pressure, and the residue was extracted with MeOH. For end group analysis, ESI-MS measurements of the methanolic extract were performed.

Coordination of DEEP. To a solution/suspension of 1 equiv of Cp_2LnX or Cp_3Ln in C_6D_6 0.5, 1, 2, or 5 equiv of a stem solution of DEEP in C_6D_6 is added, respectively. The resulting mixture is transferred into an NMR tube. ^{1}H NMR spectroscopic shifts of the formed adducts (signals of Cp and X) are determined for addition of 5 equiv of DEEP. ^{1}H and ^{31}P NMR spectroscopic shifts of coordinated DEEP are determined for addition of 0.5 equiv of DEEP, respectively. The extent of ligand exchange (Table 2) is determined from the integral ratio of the ^{1}H NMR spectroscopic signals of the cyclopentadienyl protons of formed Cp_3Ln(DEEP) and Cp_2LnX-(DEEP) for addition of 5 equiv of DEEP. For NMR spectroscopic characterization of the formed phosphonate adducts, see Supporting Information.

Activity Measurements and Kinetic Analysis. For activity measurements, the stated amount of catalyst (15−50 μmol) is dissolved/suspended in 20 mL of toluene, and the reaction mixture is thermostatted to the desired temperature. Then, the stated amount of monomer (3.5−13 mmol) is added. During the course of the measurement, the temperature is monitored with a digital thermometer, and aliquots (0.5 mL) are taken and quenched by addition to deuterated methanol (0.2 mL). After the stated reaction time, the reaction is quenched by addition of MeOD (0.5 mL). The reaction is carried out in an MBraun Glovebox under argon atmosphere to take aliquots every 6−10 s at the beginning of the measurement. For each aliquot, the conversion is determined by ^{31}P NMR spectroscopy and the molecular weight of the formed polymer by GPC-MALS analysis.

For kinetic analysis, the maximum rate is determined from the maximum slope of the conversion-reaction time plot. I^*_t is defined as the given initiator efficiency at the inflection point of the conversion-reaction time plot. In case an aliquot was taken at or sufficiently close to the inflection point the initiator efficiency determined for this aliquot is used as I^*_t; if this is not the case, I^*_t is determined as the average of the initiator efficiencies of the aliquots taken directly before and after this inflection point. The conversion used for calculation of the residual monomer concentration is determined accordingly. Error bars are calculated from the following uncertainties: $\Delta[Cat]_0$ = 0.1 mg, $\Delta[Mon]_0$ = 0.05 mL (in case of DEVP) or 0.05 g (in case of DIVP), ΔC = 3%, ΔT = 2 K, and a 5% relative uncertainty for the determination of the maximum slope and I^*_t.

■ ASSOCIATED CONTENT

Ⓢ Supporting Information

Characterization of synthesized organometallic compounds, ESI MS analysis of DAVP oligomers, detailed information for single crystal X-ray structure determination, obtained data from activity measurements and kinetic analysis. This material is available free of charge via the Internet at http://pubs.acs.org.

■ AUTHOR INFORMATION

Corresponding Author

rieger@tum.de

Notes

The authors declare no competing financial interest.

■ ACKNOWLEDGMENTS

We thank Dr. Sergej Vagin, Dr. Ning Zhang, Markus Hammann, and Dominik Lanzinger for valuable discussions. S.S. is grateful for a generous scholarship from the Fonds der Chemischen Industrie.

■ REFERENCES

(1) Ellis, J.; Wilson, A. D. *Dent. Mater.* **1992**, *8*, 79.
(2) Ebdon, J. R.; Price, D.; Hunt, B. J.; Joseph, P.; Gao, F.; Milnes, G. J.; Cunliffe, L. K. *Polym. Degrad. Stab.* **2000**, *69*, 267.
(3) Greish, Y. E.; Brown, P. W. *Biomaterials* **2001**, *22*, 807.
(4) Gemeinhart, R. A.; Bare, C. M.; Haasch, R. T.; Gemeinhart, E. J. *J. Biomed. Mater. Res., Part A* **2006**, *78A*, 433.
(5) Bock, T.; Möhwald, H.; Mühlhaupt, R. *Macromol. Chem. Phys.* **2007**, *208*, 1324.
(6) Steininger, H.; Schuster, M.; Kreuer, K. D.; Kaltbeitzel, A.; Bingoel, B.; Meyer, W. H.; Schauff, S.; Brunklaus, G.; Maier, J.; Spiess, H. W. *Phys. Chem. Chem. Phys.* **2007**, *9*, 1764.
(7) Parvole, J.; Jannasch, P. *Macromolecules* **2008**, *41*, 3893.
(8) Macarie, L.; Ilia, G. *Prog. Polym. Sci.* **2010**, *35*, 1078.
(9) Atanasov, V.; Kerres, J. *Macromolecules* **2011**, *44*, 6416.
(10) Monge, S.; Canniccioni, B.; Graillot, A.; Robin, J. *Biomacromolecules* **2011**, *12*, 1973.
(11) Salzinger, S.; Rieger, B. *Macromol. Rapid Commun.* **2012**, *33*, 1327.
(12) Seemann, U. B.; Dengler, J. E.; Rieger, B. *Angew. Chem., Int. Ed.* **2010**, *49*, 3489.
(13) Rabe, G. W.; Komber, H.; Haeussler, L.; Kreger, K.; Lattermann, G. *Macromolecules* **2010**, *43*, 1178.
(14) Salzinger, S.; Seemann, U. B.; Plikhta, A.; Rieger, B. *Macromolecules* **2011**, *44*, 5920.
(15) Zhang, N.; Salzinger, S.; Deubel, F.; Jordan, R.; Rieger, B. *J. Am. Chem. Soc.* **2012**, *134*, 7333.
(16) Zhang, N.; Salzinger, S.; Rieger, B. *Macromolecules* **2012**, *45*, 9751.
(17) Yasuda, H.; Yamamoto, H.; Yokota, K.; Miyake, S.; Nakamura, A. *J. Am. Chem. Soc.* **1992**, *114*, 4908.
(18) Chen, E. Y.-X. *Chem. Rev.* **2009**, *109*, 5157.
(19) Yasuda, H.; Ihara, E. *Macromol. Chem. Phys.* **1995**, *196*, 2417.
(20) Yasuda, H.; Ihara, E. *Adv. Polym. Sci.* **1997**, *133*, 53.
(21) Yasuda, H. *Prog. Polym. Sci.* **2000**, *25*, 573.
(22) Boffa, L. S.; Novak, B. M. *Macromolecules* **1994**, *27*, 6993.
(23) Yasuda, H.; Yamamoto, H.; Yamashita, M.; Yokota, K.; Nakamura, A.; Miyake, S.; Kai, Y.; Kanehisa, N. *Macromolecules* **1993**, *26*, 7134.
(24) Collins, S.; Ward, D. G. *J. Am. Chem. Soc.* **1992**, *114*, 5460.
(25) Collins, S.; Ward, D. G.; Suddaby, K. H. *Macromolecules* **1994**, *27*, 7222.
(26) Li, Y.; Ward, D. G.; Reddy, S. S.; Collins, S. *Macromolecules* **1997**, *30*, 1875.
(27) Sustmann, R.; Sicking, W.; Bandermann, F.; Ferenz, M. *Macromolecules* **1999**, *32*, 4204.

(28) Tomasi, S.; Weiss, H.; Ziegler, T. *Organometallics* **2006**, *25*, 3619.
(29) Giardello, M. A.; Yamamoto, Y.; Brard, L.; Marks, T. J. *J. Am. Chem. Soc.* **1995**, *117*, 3276.
(30) Nguyen, H.; Jarvis, A. P.; Lesley, M. J. G.; Kelly, W. M.; Reddy, S. S.; Taylor, N. J.; Collins, S. *Macromolecules* **2000**, *33*, 1508.
(31) Cameron, P. A.; Gibson, V. C.; Graham, A. J. *Macromolecules* **2000**, *33*, 4329.
(32) Hölscher, M.; Keul, H.; Höcker, H. *Macromolecules* **2002**, *35*, 8194.
(33) Rodriguez-Delgado, A.; Mariott, W. R.; Chen, E. Y.-X. *Macromolecules* **2004**, *37*, 3092.
(34) Ning, Y.; Cooney, M. J.; Chen, E. Y.-X. *J. Organomet. Chem.* **2005**, *690*, 6263.
(35) Rodriguez-Delgado, A.; Mariott, W. R.; Chen, E. Y.-X. *J. Organomet. Chem.* **2006**, *691*, 3490.
(36) Ning, Y.; Caporaso, L.; Correa, A.; Gustafson, L. O.; Cavallo, L.; Chen, E. Y.-X. *Macromolecules* **2008**, *41*, 6910.
(37) Frauenrath, H.; Keul, H.; Höcker, H. *Macromolecules* **2001**, *34*, 14.
(38) Hölscher, M.; Keul, H.; Höcker, H. *Chem.—Eur. J.* **2001**, *7*, 5419.
(39) Caporaso, L.; Cavallo, L. *Macromolecules* **2008**, *41*, 3439.
(40) Zhang, Y.; Ning, Y.; Caporaso, L.; Cavallo, L.; Chen, E. Y.-X. *J. Am. Chem. Soc.* **2010**, *132*, 2695.
(41) Rodriguez-Delgado, A.; Chen, E. Y.-X. *Macromolecules* **2005**, *38*, 2587.
(42) Ning, Y.; Chen, E. Y.-X. *J. Am. Chem. Soc.* **2008**, *130*, 2463.
(43) Zhang, N.; Salzinger, S.; Soller, B. S.; Rieger, B. *J. Am. Chem. Soc.* **2013**, *135*, 8810.
(44) Kaneko, H.; Nagae, H.; Tsurugi, H.; Mashima, K. *J. Am. Chem. Soc.* **2011**, *133*, 19626.
(45) Ihara, E.; Morimoto, M.; Yasuda, H. *Macromolecules* **1995**, *28*, 7886.
(46) Seemann, U. B. Ph.D. Thesis, Technische Universität München, Garching bei München, October 2010.
(47) Qian, Y.; Bala, M. D.; Yousaf, M.; Zhang, H.; Huang, J.; Sun, J.; Liang, C. *J. Organomet. Chem.* **2002**, *188*, 1.
(48) Observation of lower molecular weight fragments with $m/z = n \times M_{Mon} + M_{Na}$ has been previously observed for initiation with Cp_3Ln, and can be attributed to chain scission during ESI MS analysis as these fragments are not observed for analysis by MALDI-ToF MS.
(49) Leute, M. Ph.D. Thesis, Universität Ulm, 2007.
(50) Dengler, J. E. Diploma Thesis, Technische Universität München, Garching bei München, August 2007.
(51) Demir, S.; Mueller, T. J.; Ziller, J. W.; Evans, W. J. *Angew. Chem., Int. Ed.* **2011**, *50*, 515.
(52) Hollemann, A. F., Wiberg, E., Wiberg, N., Eds. *Lehrbuch der Anorganischen Chemie (Textbook of Inorganic Chemistry, Engl. Transl.)*; Walter de Gruyter & Co: Berlin, 2007.
(53) Birmingham, J. M.; Wilkinson, G. *J. Am. Chem. Soc.* **1956**, *78*, 42.
(54) Maginn, R. E.; Manastyrskyj, S.; Dubeck, M. *J. Am. Chem. Soc.* **1963**, *85*, 672.
(55) Evans, W. J.; Dominguez, R.; Hanusa, T. P. *Organometallics* **1986**, *5*, 263.
(56) Tilley, T. D.; Andersen, A. R. *Inorg. Chem.* **1981**, *20*, 3267.
(57) Panda, T. K.; Gamer, M. T.; Roesky, P. W. *Organometallics* **2003**, *22*, 877.
(58) Eppinger, J. Ph.D. Thesis, Technische Universität München, Garching bei München, May1999.
(59) Hultzsch, K. C.; Voth, P.; Beckerle, K.; Spaniol, T. P.; Okuda, J. *Organometallics* **2000**, *19*, 228.